



LUNG EFFGHOST V-NET: AN ENHANCED NOVEL MODEL FOR PRECISE LUNG CANCER SEGMENTATION AND DETECTION



T. Sujatha^{a,*}, P.D. Mahendhiran^b, Esther Daniel^c

^a Associate Professor, Department of AI & DS, Sri Krishna College of Engineering and Technology, Coimbatore, India

^b Associate Professor, Computer Science and Business Systems, Sri Eshwar College of Engineering, Coimbatore, India

^c Associate Professor, Division of Computer Science & Engineering Karunya Institute of Technology & Sciences, Coimbatore, India

ARTICLE INFO

Keywords:

Lung cancer detection
V-Net
Efficient- Ghost Net
Novel deep attention mechanism
Pyramid Attention Network

ABSTRACT

Accurate segmentation and detection of lung nodules in computed tomography (CT) images are essential for early diagnosis and treatment planning of lung cancer (LC). However, challenges arise due to the complex structure of lung tissue and the small, irregular shapes of nodules. This paper proposes a novel deep learning model, Lung Efficient Ghost V-Net (Lung EffGhost V-Net), which integrates the strengths of EfficientNet, GhostNet, and V-Net architectures to improve segmentation precision and detection performance. The methodology includes preprocessing with an Improved Gaussian Filter (IGF) based on a Logistic Chaotic Map to reduce noise while preserving structural details. A Novel Deep Attention Mechanism (NDAM) replaces traditional convolutional blocks with Squeeze-and-Excitation modules to enhance focus on critical features. Following segmentation, a Pyramid Attention Network (PAN) is used for multi-scale detection of lung nodules. The model is evaluated on three benchmark datasets: LIDC-IDRI, LC25000, and IQ-OTH/NCCD. Experimental results demonstrate the superiority of the proposed model, achieving 99.6% accuracy, 97.87% Dice Similarity Coefficient (DSC), and 92.05% Intersection over Union (IoU), consistently outperforming existing state-of-the-art methods. These findings confirm the potential of Lung EffGhost V-Net for accurate and robust lung cancer diagnosis in clinical settings.

1. INTRODUCTION

Abnormal cells proliferate and spread throughout the body to create cancer. The disease's precise cause is yet uncertain. Bad habits like drinking or smoking can cause it, or it can be genetic and related to the immune system. These days, the rate of technical improvement and the incidence of cancer worldwide are both rising [22]. LC is among the worst diseases in the world. LCs have a negative impact on human life and cause over 7.6 million deaths globally, according to current World Health Organization (WHO) studies. Moreover, it is anticipated to kill about 17 million people worldwide by 2030 [7]. If LC is detected early, the rate of survival after five years can rise to 54 %. Accurate segmentation of lung nodules may suggest nodule malignancy. Gross tumor volume (GTV) is also essential for systemic therapy treatment if the nodule begins to spread LC. Therefore, precise lung tumor segmentation is crucial for computer-aided diagnosis (CAD) and treatment preparation of LC. [6,25]. Nowadays, imaging techniques like computed tomography (CT) scans and biopsies are employed in diagnosis.

Probability of survival is greatly increased when LC is discovered early, or in its early stages. Consequently, numerous nations are creating early LC detection methods [20].

Although many deep learning models have been proposed for lung cancer segmentation, challenges remain due to irregular tumor morphology, imaging noise, and high false positive rates. Furthermore, previous methods often suffer from under-segmentation, insufficient multi-scale feature extraction, and lack of robustness across datasets. Hence, there is a critical need for a unified, accurate, and computationally efficient model. Radiologists have a significant obstacle while screening for pulmonary nodules because of the similarities that these nodules have with other lung tissue structures. Radiologists now find it easier and more convenient to screen for pulmonary nodules due to emergence of instruments for CAD. However, problems including high false-positive rates and poor sensitivity limit broad use of CAD systems in clinical practice [3]. Recognition of lung nodules became topic of much research in past 10 years on a variety of medical imaging techniques, like CT, low-dose CT (LDCT), magnetic resonance imaging

* Corresponding author.

E-mail addresses: sujatha@skcet.ac.in (T. Sujatha), mahendhiranpd@sece.ac.in (P.D. Mahendhiran), estherdaniell@gmail.com (E. Daniel).

(MRI), positron emission tomography (PET) and chest X-ray [19]. CT is regarded as one of the greatest imaging modalities and is now the accepted method for evaluating and studying LCs. The ability to accurately divide malignant nodules from CT scan pictures is crucial because it yields information that is closely linked to early LC detection and improves patient survival [18]. Artificial intelligence approaches appear to have been adopted by more medical professions in recent years, including dermatology, radiology, and most importantly oncology [15]. Support Vector Machine (SVM) and other machine learning (ML) approaches are utilised to regulate if nodules are malignant or benign. Although similar machine learning frameworks are used in many works, this technique's drawback is that various factors need to be modified for the system to perform correctly, which makes it challenging to replicate findings. Additionally, these systems are vulnerable due to the non-uniformity of CT scans and screening parameters. Deep training CAD systems could do end-to-end identification by identifying most important components during training [16].

Multidimensional anatomical scans and other high-dimensional data may now be examined by machines due to Deep Learning (DL) techniques. Recurrent neural network (RNN) and Convolutional neural network (CNN) are two well-known DL models regularly used for image and sequential data classification [13]. Stacked Auto Encoder (SAE), CNN, and Deep Neural Network (DNN) are three main DL structures for cancer diagnosis. CNN produced the best outcomes when associated to DNN and SAE [2,8]. U-Net, which uniformly uses a variety of up and down sampling techniques to uncover an object's semantic and visual characteristics, is the most widely used DL approach. It can segment objects with great flexibility and effectiveness. Additionally, based on this approach, optimization techniques such as attention block, dilated convolution, residual block, and dense connection have gradually emerged and produced positive results in automated segmentation of tumors. Although a number of studies have sought to segment lung lesions and have obtained credible results, there is still potential for improvement in their effects [5,24].

The major contribution of this work are as follows:

- The novel model Lung EffGhost V-Net is proposed that integrates GhostNet, EfficientNet, and V-Net architectures for precise segmentation and recognition of LC in CT images.
- The introduction of a modified MBConv block by replacing standard convolutional layers with Ghost modules, improving computational efficiency without sacrificing accuracy.
- The advanced Gaussian filtering technique is employed incorporating a Logistic Chaotic Map for better noise reduction while retaining critical features like edges and textures.
- The new attention mechanism using Squeeze and Excitation (SE) blocks is introduced to focus on critical lung nodule features while reducing the influence of background noise.
- The Pyramid Attention Network (PAN) is introduced for multi-scale feature extraction, enabling effective recognition of lung nodules of varying sizes and shapes.

The framework of the paper is as follows: In [Section 2](#), a summary of relevant studies is provided. In [Section 3](#), the proposed method is reviewed. [Section 4](#) provides a summary of the findings. The paper's conclusion is presented in [Section 5](#).

2. LITERATURE REVIEW

This section reviews some of the most recent research works regarding lung cancer detection and segmentation using DL techniques.

Cifci [4] proposed a new segmentation approach for LC from CT images using SegChaNet, compared its performance with U-Net and V-Net. The proposed approach combines CAM into U-Net framework to robustly segment chest regions away from lung areas affected by cancer. For achieving this, SegChaNet uses a number of encoders to encode

input CT scan information into feature maps. This has featured a specially designed multiscale dense-feature extraction module, which would now enable intricate details from the encoded feature maps for precise and robust segmentation.

Tsivgoulis et al. [21] have presented SqueezeNodule-Net, a light-weight and accurate CNN that requires only a moderately powerful computer system to quickly categorize nodules as benign or cancerous. It is based on the Fire Module and SqueezeNet, a small CNN model whose structure we changed in two distinct ways and contrasted with the most advanced models. Two models, SqueezeNodule-Net V1 and SqueezeNodule-Net V2, were suggested in this work. A condensed form of the original SqueezeNet, these variants can operate at respectably fast speeds on mid-range computers.

Naseer et al. [14] proposed a modified U-Net-based three-stage model for classification of LC. First stage processes a CT slice by segmenting lung lobes by means of a modified U-Net. The second stage uses another modified U-Net to identify candidate nodules based on labels and predicted masks. Lastly, the third stage utilizes an SVM to categorize identified nodules as cancerous or non-cancerous with improved accuracy in categorizing LC. A modified version of AlexNet serves as its foundation. Using the publicly available LUAN16 dataset, the investigational findings of the suggested procedure for LC classification, candidate nodule extraction, and lobe segmentation have demonstrated encouraging outcomes.

Youssef et al. [23] utilized a two-level joint Markov-Gibbs random field (MGRF) model for precise delineation of lung area and distinction of lung wall nodules. Subsequently, a DL U-Net strategy was adopted to delineate region of interest (ROI) with lung nodules by diminishing involvement of surrounding tissues. More significant improvement happened with a 3D U-Net that learned from a new loss function and thereby solved under- and over-segmentation problems to better segment the nodule. LAFCE was created, a novel adaptive loss function that helps avoid over- or under-segmenting the lung nodules that were found. The model's outstanding performance on LIDC/IDRI database and locally collected dataset proves its high level of accuracy, repeatability, and generalisability in lung nodule segmentation.

Bhattacharyya et al. [1] have established a condensed kind of the Debnath Bhattacharyya-Network (DB-NET) architecture made for lung nodule segmentation. A modified U-NET design, effective for lung nodule segmentation (DB-NET) was demonstrated in paper using a weighted bidirectional feature network. The model's foundation is the U-Net architecture, which gathers and decodes feature maps. A feature enricher called the Bi-FPN blends features from various scales. The findings were examined and presented, and the proposed approach successfully segmented lung nodules with 88.89 % dice similarity coefficient for the LUNA16.

Mahum and Al-Salman [12] introduced Lung-RetinaNet as a highly efficient LC detection system based on RetinaNet. It integrates a multi-scale feature fusion module that aggregates the network layers to enhance semantic information in deep prediction layers. A lightweight context module also integrates contextual data at every stage of the network, enhancing feature representation to allow accurate identification of small tumours with higher efficiency and precision.

Ji et al. [10] proposed ELCT-YOLO, a one-stage efficient model for lung tumor detection in CT scans. This model embodies specially designed neck structures to further improve multi-scale representation of the feature layers without having an extra complex feature fusion network or a deeper backbone. Additionally, ELCT-YOLO proposes a new Cascaded Refinement Scheme of two different Receptive Field Enhancement Modules, denoted as RFEM. These modules finally handle the problem of lacking receptive fields after decoupling: improving the model's capability to capture multi-scale context information, thus realizing the broader effective receptive field and greatly improving the accuracy and efficiency of tumor detection achieved by ELCT-YOLO.

Imran et al. [9] have intended to improve the classification accuracy of histological images of non-small cell LC (NSCLC) by putting forth a

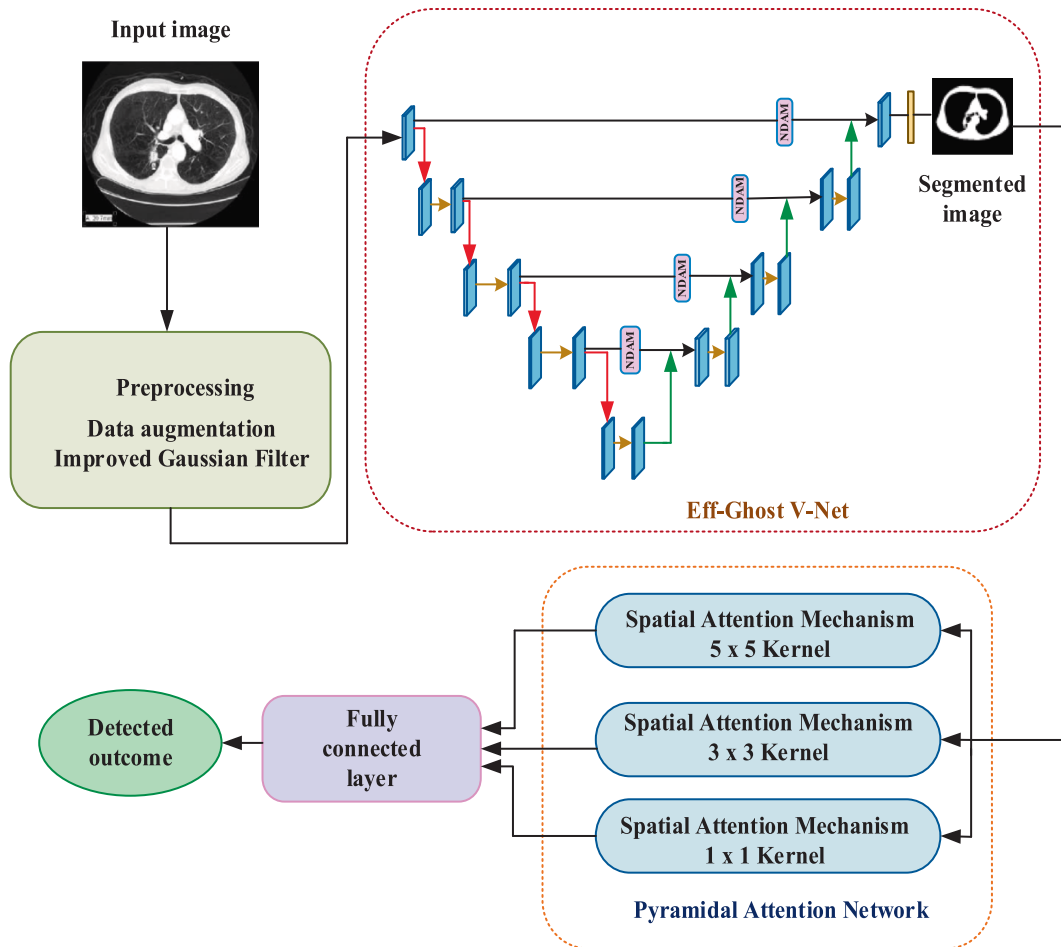


Fig. 1. The overall block diagram of the proposed architecture.

unique deep-learning architecture that combines vision transformers (ViTs) with convolutional neural networks (CNNs). NSCLC is divided into three groups by the model: squamous cell carcinoma, adenocarcinoma, and normal. ViTs are used to comprehend long-range relationships between picture patches, whereas CNNs are utilized to collect local characteristics. The LC25000 dataset, a reference dataset for the categorization of NSCLC histopathology images, was used to train and evaluate our model.

Ji et al. [11] introduced ResDSda_U-Net, an advanced neural network built upon the U-Net architecture with significant enhancements for improved performance. First, it introduces the ResDS block, which combines a Depthwise Over-parameterized Convolutional layer (DO-Conv) with a parameter-free attention module (SimAM) to enhance feature extraction. Second, a Dense Atrous Spatial Pyramid Pooling (DASPP) module is added between the encoder and decoder, using modified dilation rates to extract multi-scale features more effectively. Third, channel and spatial attention mechanisms are integrated into the decoder through newly designed Convolution and Channel Attention (CCA) and Convolution and Spatial Attention (CSA) blocks. These components boost global pixel attention, capture contextual information, and refine the decoder's pixel elimination process.

Raza et al. [17] introduced Lung-EffNet, a novel transfer learning-based predictor in 2023 for LC classification, building on the EfficientNet architecture but with additional top layers in the head of the classification for higher performance. The approach is tested by the model through five versions of EfficientNet, namely B0–B4, using the benchmark dataset “IQ-OTH/NCCD” that categorizes patients into benign, malignant, or normal based on LC presence. The employed data augmentation techniques resolve the problem of class imbalance and

provide more balanced training to the model. Lung-EffNet has shown results with accurate and reliable classification for LC, using the powerful feature extraction capabilities of EfficientNet and overcoming some biases via robust pre-processing and augmentation strategies.

LC diagnosis and segmentation are two examples of such challenging tasks where boundaries are blurred in most CT images due to complex surrounds and irregular lung nodule forms. There is a huge necessity to find nodules accurately in early diagnosis, planning of treatment, and surgery. Deep learning models have encountered issues like class imbalance, under- or over-segmentation, and inefficient computation for existing models. The proposed study contains the innovative segmentation and detection model integrating EfficientNet, GhostNet, and advanced attention mechanism in a V-Net framework. The proposed model would overcome the challenges here and improve segmentation precision, improve multi-scale features, and achieve superior classification performance for diverse LC datasets.

While prior studies have utilized CNN variants, modified U-Net architectures, or attention blocks independently, none have effectively combined lightweight modules like GhostNet and EfficientNet with encoder-decoder architectures in a V-Net framework. Moreover, most models lack robust attention mechanisms to suppress background noise and highlight relevant nodule features. Our proposed Lung EffGhost V-Net addresses these limitations through integrated architectural innovations and multi-level attention mechanisms, ensuring superior performance across diverse datasets.

3. PROPOSED METHODOLOGY

The proposed methodology in this paper introduces a novel model

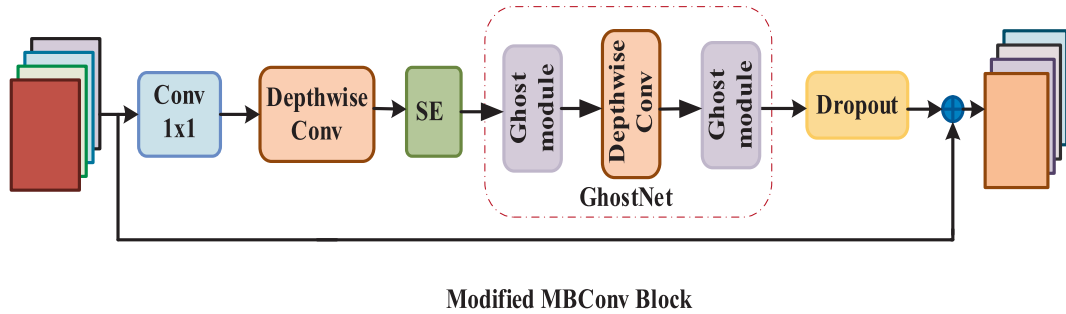


Fig. 2. The Modified MBConv block structure.

called Lung EffGhost V-Net aimed at enhancing LC segmentation and detection using CT images. This approach is designed to overcome challenges related to the irregular shapes of lung nodules and complex backgrounds that obscure accurate segmentation. To achieve this, the Lung-EffGhost V-Net combines the power of multiple architectural elements: GhostNet, Efficient Net, and V-Net, enhanced by a novel deep attention mechanism (NDAM) and advanced noise reduction techniques. This integration targets precise segmentation, enabling the detection of lung nodules at varying scales. The overall block diagram of the proposed Lung Eff-Ghost V-Net is depicted in the Fig. 1.

3.1. Data collection and preprocessing

The model is trained on three datasets (LIDC-IDRI, LC25000, and IQ-OTH/NCCD). LIDC-IDRI dataset comprises annotated lung CT scans to help in acting as ground truth for the intended tasks of segmentation and classification. The large pool of labelled medical images – LC25000 – comprises LC CT scan images that are sufficient to train DL models. IQ-OTH/NCCD dataset, including detailed annotations of benign and malignant cases to efficiently support classification. All datasets combined capture a wide range of nodule characteristics as well as variations in CT images, thereby enhancing generalizability of model and improving its presentation. Once collected, the data undergoes preprocessing, which include data augmentation such as flipping, rotation and cropping to increase training samples in the datasets and to reduce noise IGF is employed. To ensure compatibility across the three datasets, all CT images were resized to a uniform size of 256×256 pixels and converted to grayscale PNG format. Normalization was performed to scale intensity values between 0 and 1.

3.1.1. Data augmentation

A variety of transformations such as flipping, rotation and cropping are utilized to augment the dataset. These techniques help to create variations of the original images, providing the model with more diverse examples to learn from. These transformations are applied to artificially expand the training data, thereby enhancing the model's generalization ability. They simulate different orientations and variations of nodules, reducing overfitting and improving robustness in real-world clinical scenarios.

Flipping: Flipping the image can be done in an upward direction or on a level plane. It creates an image by rotating it by a factor of 90 degrees. Vertical flipping is not supported by all systems. The photo is first rotated 180 degrees to refine vertical flipping, and then level flipping is carried out.

Cropping: The process of resizing a small portion of an original image to match its dimensions is known as random cropping. If necessary, the image is resized using random cropping. Translation preserves the spatial dimensions of an image, as opposed to arbitrary cropping, which reduces their size.

Rotation: The image can be oriented at small angles or rotated 90 degrees, depending on the needs. After an image has been aligned, it is rotated 90 degrees without any background noise added. When angled

slightly, however, this is not the case. If the backdrop of the image is white or black, the newly added noise will be absorbed by the image. The network will recognise it as a component of the image and prevent it from fully blending in if the backdrop of the image has distinct colours.

3.1.2. Improved Gaussian filtering (IGF)

The augmented images of the LC are fed into the IGF that enhances the segmentation and detection of LC by reducing noise adaptively while preserving edges and textures. It uses a Logistic Chaotic Map to adjust smoothing dynamically for noise at different levels, ensuring details and boundaries of tumours are preserved. This produces LC images that are clearer and more detailed, which will help the input models produce high-quality segmentation. For a LC diagnosis to be made correctly, the precision of IGF facilitates the precise delineation and feature extraction of a tumour. The Gaussian filter is selected due to its efficiency in reducing Gaussian noise while preserving edge information critical for medical diagnosis. Its smoothing capability helps to enhance image quality without blurring essential tumor boundaries.

Gaussian filters are frequently employed to denoise images because they create a linear combination of neighbouring values by convolving the image with a constant matrix. A narrower frequency domain promotes smoothness and reduces low frequencies by expanding the filter's spatial domain. A Logistic Chaotic Map (LCM), which adds a dynamic and adaptive component to the smoothing process, is included into an improved version of Gaussian filtering to increase its denoising efficiency. The enhanced version of Gaussian filter with Logistic Map as indicated by Eq. (1),

$$G_o(x, y) = \frac{1}{2\pi\sigma^2} e^{-\frac{(x^2+y^2)}{2\sigma^2}} + L_M \quad (1)$$

$$L_M = \mu d_t(1 - d_t) \quad (2)$$

Where L_M is the Logistic chaotic map and Controlled variability is introduced by L_M , where d_t is a dynamic parameter in the chaotic sequence and μ , usually set to 4, ensures maximal chaotic behavior. The output of the chaotic map scales dynamically within the range of (0,1).

The LCM introduction of non-linearity and adaptivity helps in having differential responses to the noise intensities across the image that maximize enhanced noise reduction, particularly in complex scenarios such as medical imaging, while it keeps maintaining critical features like edges and fine textures by adjusting the smoothing weight according to local variations. The operational mechanism combines the stable mechanism of the Gaussian smoothing term with the adaptability mechanism of the chaotic map for iterative adjustment of local pixel values. The result is superior noise suppression, even in the presence of high-intensity noise, and better detail retention than standard Gaussian filtering.

3.2. Lung EFF-Ghost v-net for segmentation

The proposed algorithm follows a systematic pipeline for effective

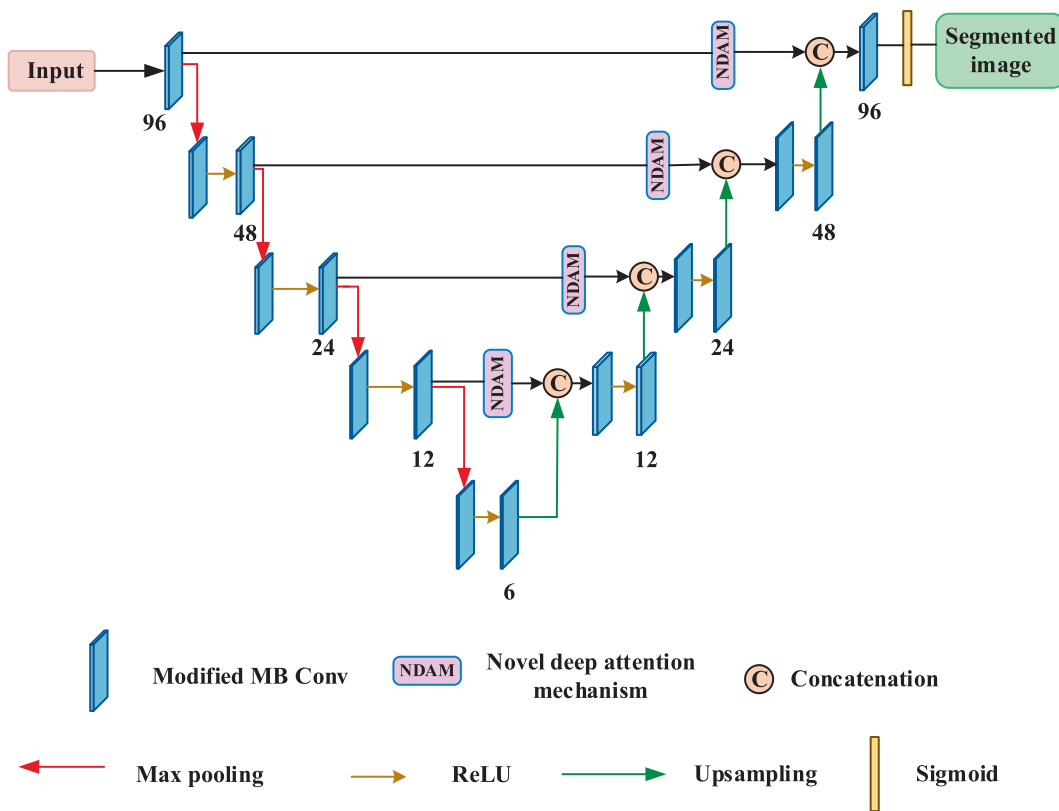


Fig. 3. The Lung Eff-Ghost V-Net architecture.

lung nodule segmentation and detection. First, the CT images undergo preprocessing including data augmentation (flipping, cropping, and rotation) and noise reduction using the Improved Gaussian Filter (IGF). Second, the preprocessed images are passed into the encoder of the V-Net, composed of modified MBConv blocks where the standard convolutions are replaced by Ghost modules. These layers extract semantic features while preserving computational efficiency. Third, skip connections transfer spatial details from encoder to decoder, which is also constructed with Ghost-augmented MBConv blocks. A Novel Deep Attention Mechanism (NDAM) is applied in the decoder to suppress irrelevant background and enhance relevant features. Finally, the segmented outputs are passed to the Pyramid Attention Network (PAN), which performs multi-scale feature analysis to accurately classify lung nodules of varying shapes and sizes. This architecture ensures both fine-grained segmentation and high-precision detection. Structure of Modified MBConv is shown in the Fig. 2.

The conventional MBConv structure includes of a sequence-and-exception (SE) module, a dropout layer, a depth-wise convolution, and a 1×1 convolution for dimension reduction. Only BN operations are carried out by the second 1×1 convolution, whereas BN and Swish activation processes follow the first 1×1 convolution and Depth wise Conv convolution. This work substitutes the convolution in the MBConv block with the ghost module in the GhostNet, which is used after the SE block. GhostNet introduces a new Ghost module that uses low-cost operations to generate additional feature maps. With fewer computations and parameters, this novel neural network building block efficiently generates more feature maps. There are two components to this module's implementation. First, GhostNet builds feature maps with fewer channels using a traditional convolutional calculation. It then generates additional feature maps using a low-cost process. Lastly, it creates a new output by concatenating several feature maps.

Ghost bottleneck modules in Ghost Net are divided into two categories according to stride. When stride is 1, the structure of the Ghost bottleneck module is composed of two Ghost modules and is represented

using normal residuals. The first module acts as an extension layer to add more channels. The second module links the inputs and outputs of these two Ghost modules by using the shortcut after reducing the number of channels to match the shortcut path. Ghost bottleneck module maintains its structural characteristics when stride = 1 and has the layout of a traditional bottleneck module when stride = 2. This method reduces the amount of computation needed for a lightweight two-dimensional depth-wise convolution by utilising MobileNetv2's expertise. After every layer in the module design process, batch normalisation (BN) and the ReLU nonactivation function are used. This Ghost module of stride 2 is utilized in the standard MBConv block. This Modified MBConv block is used as the baseline of the proposed model as an encoder and decoder of the V-Net in the proposed architecture. The integration of EfficientNet, GhostNet, and V-Net is strategically designed to optimize both performance and computational efficiency. EfficientNet enables compound scaling of depth, width, and resolution, improving feature extraction while maintaining low parameter counts. GhostNet complements this by generating more feature maps using cheaper operations, significantly reducing redundancy in convolution layers. Meanwhile, the V-Net architecture ensures spatial consistency and effective learning of volumetric information via its encoder-decoder structure with skip connections. This synergy offers a lightweight yet highly accurate framework suited for clinical and resource-constrained environments. The encoder processes the input images by successive down sampling through a sequence of modified MBConv blocks each coupled with a max-pooling layer. At such time of down sampling, the encoder will derive the high-level semantic features that become important to identify various structures in an image. Decoder ends with the upampling of encoded feature maps to reconstruct them back to the size of the original image. The encoder maintains spatial consistency with skip connections as it enhances detailed retention. Such information flowing directly from earlier layers into corresponding decoder layers improves its ability to retain detail. The novel deep attention mechanism (NDAM) is employed by the decoder to further refine the output of segmentation by focusing

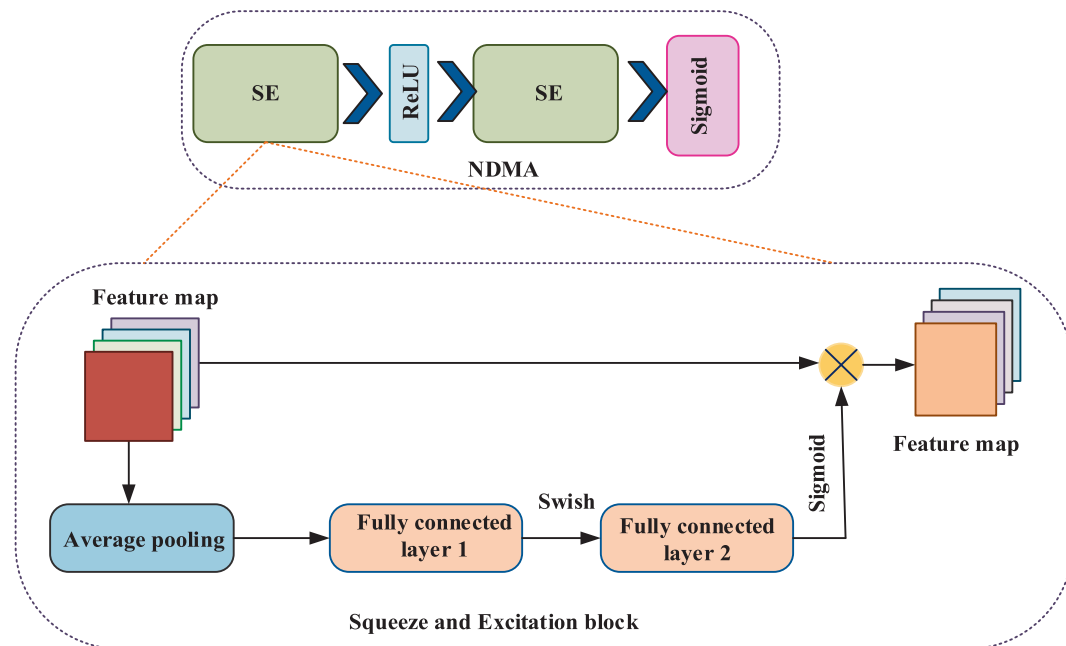


Fig. 4. NDAM architecture.

on relevant nodule features and by suppressing background noise. This architecture of an encoder-decoder attains a balance between the extraction of complex features that keep accurate spatial reconstruction in order to ensure improved performance in terms of segmentation. The Lung Eff-Ghost V-Net architecture is depicted in the Fig. 3.

The NDAM is an essential component of the Lung-EffGhost V-Net architecture, enhancing its capability to focus on critical nodule features in lung segmentation and detection within CT images. NDAM operates by directing attention to the most relevant features while reducing the influence of unnecessary background information. For the NDAM, the standard convolution block in the attention mechanism is replaced with the SE block. The process begins with input of a feature map generated by the convolutional layers in the encoder or decoder of the V-Net, which captures the spatial details of an image. Two completely linked layers, a Sigmoid activation function, and global average pooling make

up the SE module that is utilised. Furthermore, between the two complete connection layers, the Swish activation mechanism is introduced. An input image that is $H \times W \times C$ is stretched into $1 \times 1 \times C$ using global pooling and fully connected layers, and then multiplied by the original image to apply weight to each channel. The network may therefore learn additional feature information due to the SE module. At the core of NDAM lies Squeeze and Excitation (SE) block, an expression of channel-wise dependencies in two steps. First, the global average pooling of spatial dimensions is used to perform the squeeze operation, resulting in a single vector per channel that contains global information. This vector now advances into the excitation phase, wherein, in a sequence of two fully connected layers separated by Swish activation, it further provides channel-wise weights through the Sigmoid function. These weights modulate the relative importance of the channels in the original feature maps, such that features that are less relevant will selectively high-

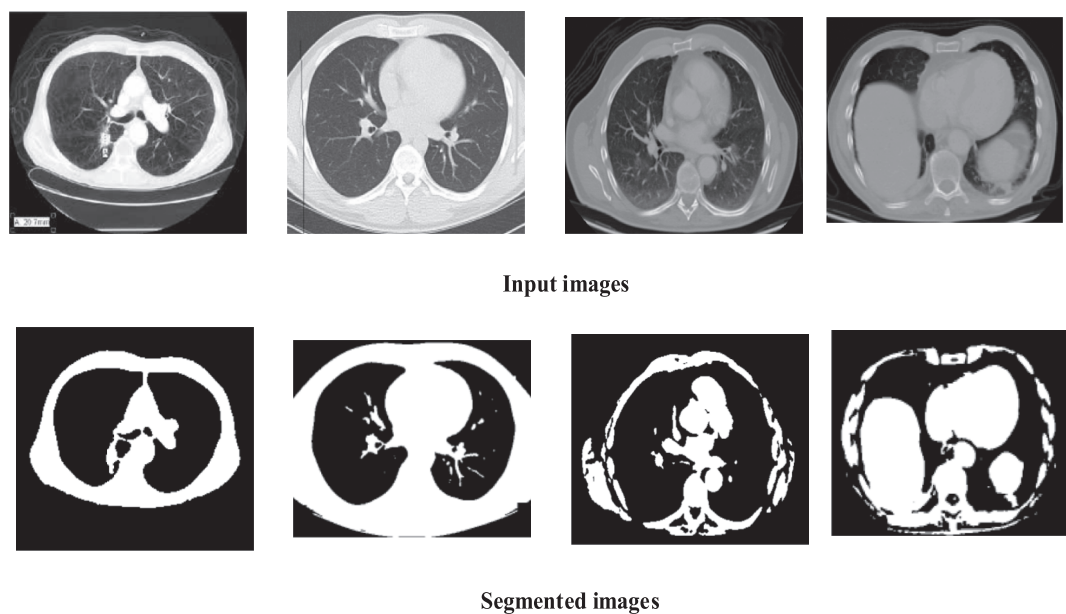


Fig. 5. Segmented images.

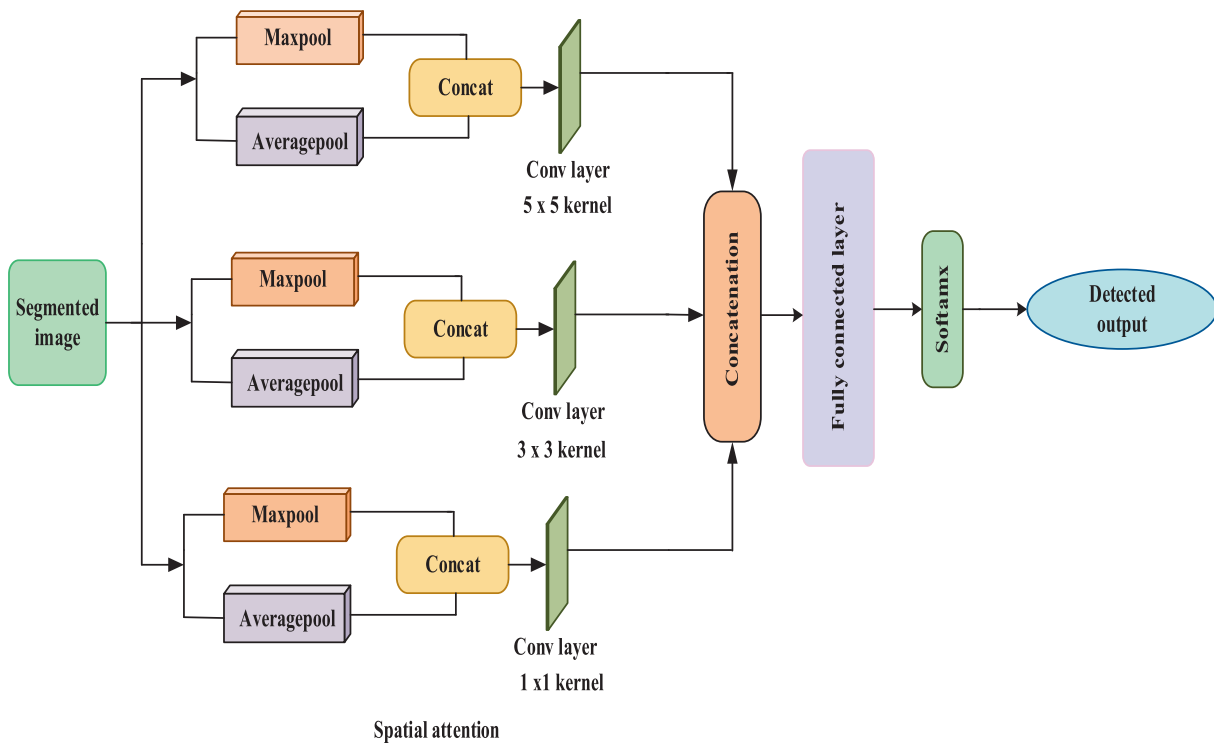


Fig. 6. Pyramidal Attention Network architecture.

lighted or suppressed. These refined outputs are now fed to the next layers of the network, with every stage's feature map being focussed more and more on the information concerned with relevant nodular information, hence aiding in effective segmentation and detection. Fig. 4 illustrates the NDAM architecture.

NDAM brings attention to important features of lung nodules; therefore, it allows the model to differentiate nodule structures from background tissues effectively, improving the performance of segmentation. Although NDAM introduced computations, attention is usually confined to the most informative regions. This adaptive channel-wise attention of NDAM enabled Lung-EffGhost V-Net to capture important information with noise minimized, thus its precision and performance in the complicated task of detecting LC were very much elevated. It applies a 1×1 convolution on the last up sampled features, which is the segmentation map, and then uses sigmoid activation to map each pixel into the probability range $[0,1]$, which is necessary for probabilistic segmentation. The loss function has a crucial effect on CNN's performance. Because nodule region only covers a small area, it can cause loss function to drop sharply to local minimum during training, can lead to a large segmentation deviation in medical image segmentation. The segmentation deviation brought on by an uneven nodule region and backdrop can be successfully reduced by dice loss (DL), which processes unbalanced datasets well. Equation (3) defines the DL .

$$DL(y, \hat{p}) = 1 - \frac{2y\hat{p} + 1}{y + \hat{p} + 1} \quad (3)$$

where the numerator and denominator are both increased by 1 to guarantee function is not indeterminate in edge case situations, like when $y = \hat{p} = 0$. Fig. 5 depicts the sample input and segmented images. The segmented LC's images are sent to the Pyramidal Attention Network.

3.2.1. Training Configuration

The model was implemented using MATLAB 2023a and trained over 100 epochs. The Adam optimizer was used with an initial learning rate of 0.0001. A batch size of 16 was maintained throughout the training.

The Dice loss function was employed due to its effectiveness in handling imbalanced segmentation tasks, especially where nodule regions are sparse.

3.3. Pyramidal attention network for detection

The Pyramidal Attention Network now receives the segmented images. To improve lung nodule identification, the Pyramidal Attention Network processes the segmented images from the Lung EffGhost V-Net. PAN incorporates multi-scale feature fusion to capture fine-grained and background information. An attention mechanism overpowers inessential information while giving priority to important nodular characters. By increasing detection accuracy, refined feature maps make it possible to identify nodules with irregular forms and a range of sizes. This multi-scale method ensures accurate and reliable detection in intricate lung structures.

The proposed architecture makes use of a multi-scale feature extraction approach in combination with spatial attention, effectively used to categorize lung nodules from segmented CT images. Fig. 6 illustrates Pyramidal Attention Network architecture.

First, the CT image is segmented to identify regions of interest, such lung nodules. Average pooling focusses on micro characteristics like texture and intensity, whereas max pooling captures coarse information connected to the overall shape. To combine local and global data, these pooled feature maps are concatenated along channel dimension. The map is then activated using a sigmoid function for classification after convolution layers have extracted key features and suppressed irrelevant data.

$$F_{Concat} = CONCAT[maxpool(F_{in}), avgpool(F_{in})] \quad (4)$$

where $CONCAT$ stands for the outcomes of connecting maximum pooling and global pooling, $maxpool$ and $avgpool$ for maximum pooling and global pooling, respectively, and F_{in} for input frame difference map. The Conv layer processed the input feature maps in three different ways. From top to bottom, the convolutional kernel sizes in the convolution layer were 5, 3, and 1. The number of channels decreased as the

convolutional kernel size increase, creating an inverted pyramidal structure for the convolutional kernel size and a positive pyramidal structure for the number of channels. The concatenated feeds into an inversion pyramid structure of convolutional layers with kernel sizes progressively smaller: 5x5, 3x3, and 1x1. The refined features are flattened and processed by a fully connected layer, which learns complex feature relationships before being passed through a SoftMax layer to compute class probabilities. The class with highest probability is assigned as detected output. Detected output represents the predicted class labels related to LC.

The above proposed architecture decreases spatial dimensions of feature maps at cost of depth and allows increasingly more complex features to be captured at layers deeper in the network.

4. RESULT AND DISCUSSION

The experiment outcomes are discussed in this part utilizing assessment measures including Sensitivity, F-measure, Matthews Correlation Coefficient (MCC), accuracy, Specificity, Recall, False Negative Ratio (FNR), F1-score, Negative Predictive value (NPV), precision, and False Positive Ratio (FPR) for proposed Lung Eff-Ghost V-Net for LC detection. MATLAB is used to implement the proposed model. The evaluation outcomes are compared to the various existing techniques such as Seg-ChaNet, Modified U-Net, Lung EffNet and the proposed Lung Eff-Ghost V-Net. This work performs a comprehensive comparative evaluation with existing state-of-the-art models using extensive metrics across three datasets, providing a robust and in-depth performance analysis.

4.1. Dataset description

Dataset 1: LIDC-IDRI dataset: (<https://www.kaggle.com/dataset/s/zhangweiled/lidcidri>) Computer-aided diagnosis (CAD) consists of lung CT images and annotated lesions, is used to develop and assess these LC approaches. The LIDC-IDRI dataset consists of 1,018 CT scans from 1,010 patients. Among these, approximately 7,371 nodules have been annotated by four experienced radiologists. Four highly skilled thoracic radiologists independently annotated each image, labelling lesions as “nodule > or = 3 mm,” “nodule < 3. mm,” or “non-nodule > or = 3 mm.”

Dataset 2: LC25000 dataset: (<https://www.kaggle.com/datasets/andrewmvd/lung-and-colon-cancer-histopathological-images>) This dataset includes 15,000 lung images equally divided into three classes: benign, malignant, and normal (5,000 images per class). Each image is in the JPEG file format and has a size of 768 × 768 pixels. The images, which included 750 total images of lung tissue and 500 total images of colon tissue, were extracted from a preliminary sample of verified and HIPAA-compliant sources.

Dataset 3: IQ-OTH/NCCD – Lung Cancer Dataset: The LC dataset from the Iraq-Oncology Teaching Hospital/National Center for Cancer Diseases (IQ-OTH/NCCD) (<https://www.kaggle.com/datasets/adityamahimkar/igothnccd-lung-cancer-dataset>) was collected at the mentioned speciality hospitals throughout a three-month period in the autumn of 2019. It includes CT scans of both healthy people and LC patients at different stages. It contains 1,190 CT scan slices from 110 patients, categorized as: 40 malignant, 15 benign, and 55 normal cases. These situations fall into one of three categories: malignant, benign, or normal, or. 40 of these instances have been found to be malignant, fifteen to be benign, and 55 to have normal features. The CT scans were first collected in DICOM format.

4.2. Performance metrics

Performance Metrics employed to evaluate proposed model are given below,

(i) **Accuracy:** It is calculated as ratio of successfully recognised samples to all samples.

$$\text{Accuracy} = \frac{TP + TN}{TP + TN + FP + FN} \quad (5)$$

(ii) **Precision:** The precision metric quantifies proportion of samples properly recognized as positive among all samples predicted to be positive.

$$\text{Precision} = \frac{TP}{TP + FP} \quad (6)$$

(iii) **Sensitivity:** Percentage of true positive samples were correctly classified as positive is measured by sensitivity.

$$\text{Sensitivity} = \frac{TP}{TP + FN} \quad (7)$$

(iv) **Specificity:** Specificity is determined by how many actual negative samples are correctly categorised as negative.

$$\text{Specificity} = \frac{TN}{TN + FP} \quad (8)$$

(v) **F-Measure:** It is the harmonic mean of precision and recall.

$$F - \text{Measure} = \frac{2 * \text{precision} * \text{recall}}{\text{Precision} + \text{recall}} \quad (9)$$

(vi) **FPR:** FPR determines percentage of actually negative samples were incorrectly categorised as positive.

$$FPR = \frac{FP}{FP + TN} \quad (10)$$

(vii) **FNR:** It calculates proportion of true positive samples were incorrectly classified as negative.

$$FNR = \frac{FN}{TP + FN} \quad (11)$$

(viii) **MCC:** MCC spans from -1 to +1 and integrates data regarding true and false positives and negatives into a single value, where +1 denotes a perfect classification, 0 denotes random categorization, and -1 denotes the full discrepancy between prediction and observation.

$$MCC = \frac{((TP * TN) - (FP * FN))}{\sqrt{((TP + FP) * (TP + FN) * (TN + FP) * (TN + FN))}} \quad (12)$$

(ix) **NPV:** It determines the proportion of actual negative samples that were accurately classified as such out of all potentially negative samples.

$$NPV = \frac{TN}{TN + FN} \quad (13)$$

(x) **IoU:** The IOU value indicates how comparable the ground scene region of the objects in the set of images is to the forecast region.

$$IoU = \frac{TP}{FP + TP + FN} \quad (14)$$

(xi) **DSC:** A statistical measure for comparing the similarity of two samples is called the DSC. The DSC, which is defined as the measurement of the spatial overlap between two segmentations, A and B target regions,

$$DSC = \frac{2|A \cap B|}{A + B} \quad (15)$$

where False Positives (FP) is amount of negatively classified samples that were incorrectly classified, False Negatives (FN) is amount of positively categorised samples that were incorrectly classified, True Positives (TP) is amount of positively categorised samples that were correctly categorised, True Negatives (TN) is amount of negatively classified samples that were correctly classified.

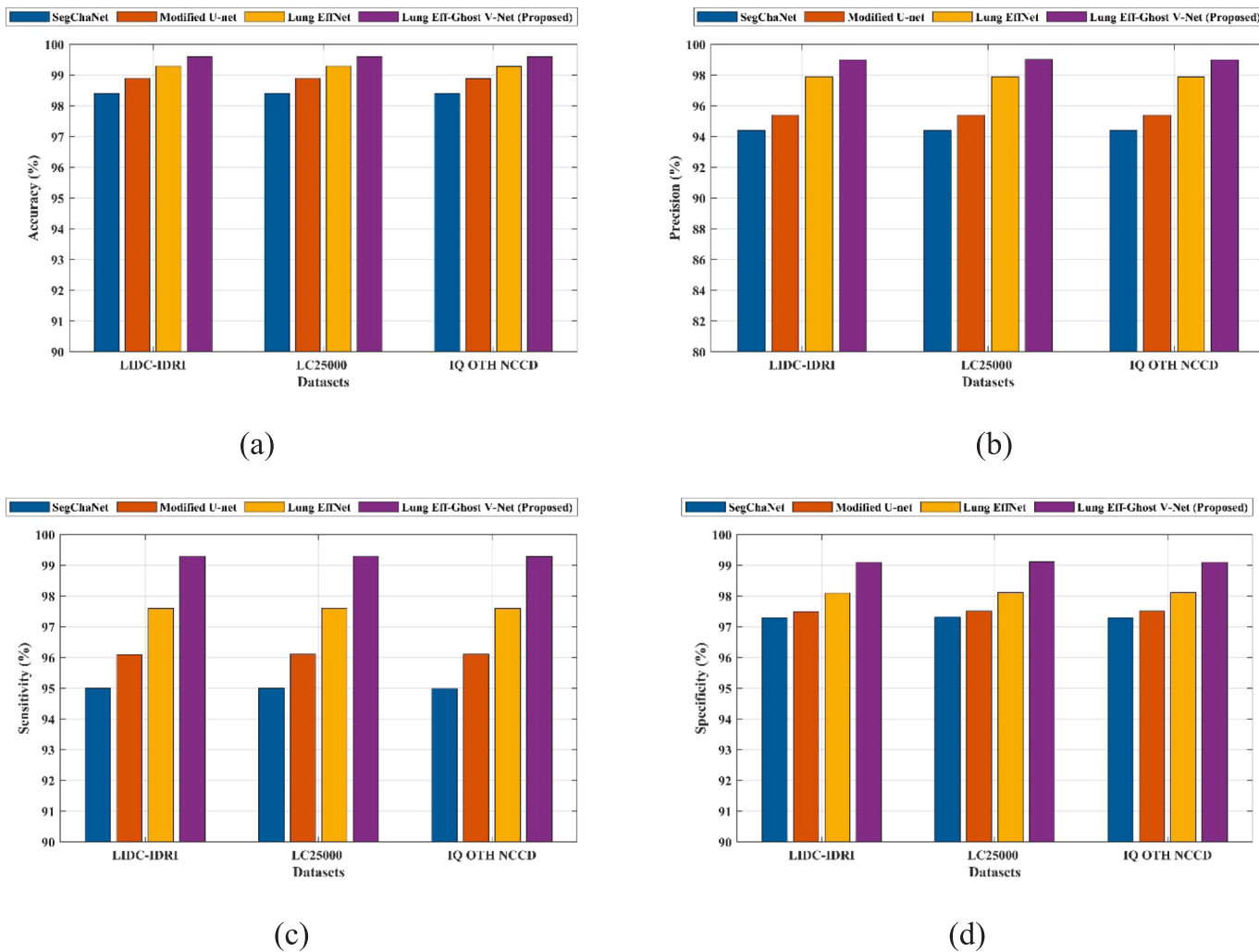


Fig. 7. Performance evaluation of (a) Accuracy, (b) Precision, (c) Sensitivity, (d) Specificity.

4.3. Performance analysis of the proposed model for different datasets

Three datasets used for LC detection LIDC-IDRI dataset (Dataset 1), LC25000 dataset (Dataset 2), and IQ-OTH/NCCD-Lung Cancer Dataset (Dataset 3) are used to perform performance analyses on different models. Fig. 7(a)-(d) provide the graphical analysis for the different performance measures, such as precision, specificity, accuracy, and sensitivity.

The proposed Lung EffGhost V-Net has improved efficiency over the existing models, namely, SegChaNet, Modified U-Net, and Lung EffNet, in three datasets: LIDC-IDRI, LC25000, and IQ-OTH/NCCD. For LIDC-IDRI dataset, it attained an accuracy of 99.6 %, in which its high performance drowns that of SegChaNet with a value of 98.4 %, Modified U-Net with the value of 98.9 %, and Lung EffNet with a value of 99.3 %. Therefore, the network shows exceptional capability for the accurate segmentation as well as detection of lung nodules from CT scans. On LC25000 dataset, model was able to hit an accuracy of 99.61 %, which was over the 98.41 % SegChaNet, 98.9 % Modified U-Net, and 99.3 % Lung EffNet respectively that prove how tough it is in the execution of histopathological images concerning the detection of LC. In IQ-OTH/NCCD, the Lung EffGhost V-Net with 99.6 % accuracy stands out, effectively outperforming SegChaNet with 98.41 %, Modified U-Net with 98.89 %, and Lung EffNet with 99.29 %, thereby significantly making it effective in handling diverse clinical real-world CT scans. For the LIDC-IDRI dataset, the Lung EffGhost V-Net achieves the highest precision of 99 %, outperforming SegChaNet, Modified U-Net, and Lung

EffNet, showcasing its exceptional ability to minimize false positives during the segmentation and detection of lung nodules in CT scans. On LC25000 dataset, it maintains its lead with a precision of 99.01 %, significantly surpassing other existing models demonstrating its robustness in identifying true positive cases in histopathological images while avoiding irrelevant features. Similarly, for the IQ-OTH/NCCD dataset, the Lung EffGhost V-Net achieves a precision of 99 %, underscoring its effectiveness in accurately distinguishing lung nodules from non-nodule structures in diverse clinical CT scans.

For the LIDC-IDRI dataset, the proposed Lung EffGhost V-Net achieves the highest sensitivity of 99.3 %, surpassing SegChaNet of 95 %, Modified U-Net of 96.1 %, and Lung EffNet of 97.6 %, showcasing its ability to detect true positive cases with minimal false negatives in lung nodule segmentation and detection. Similarly, on the LC25000 dataset, it leads with a sensitivity of 99.3 %, outperforming SegChaNet of 95 %, Modified U-Net of 96.11 %, and Lung EffNet of 97.61 %, demonstrating its robustness in accurately identifying true positive cases in histopathological images. For the IQ-OTH/NCCD dataset, the Lung EffGhost V-Net achieves a sensitivity of 99.29 %, surpassing other existing methods. The proposed Lung Eff-Ghost V-Net has a specificity of 99.1 %, which is higher than that of the others such as SegChaNet at 97.3 %, modified U-Net at 97.5 %, and Lung Eff-Net by 98.1 %. Similarly, for the LC25000 dataset, it also led by having a specificity of 99.11 %, surpassing the subsequent: SegChaNet at 97.31 %, modified U-Net by 97.51 %, and Lung Eff-Net at 98.11 %. For the IQ-OTH/NCCD dataset, the Lung Eff-Ghost V-Net also outperformed all other models with 99.11 %

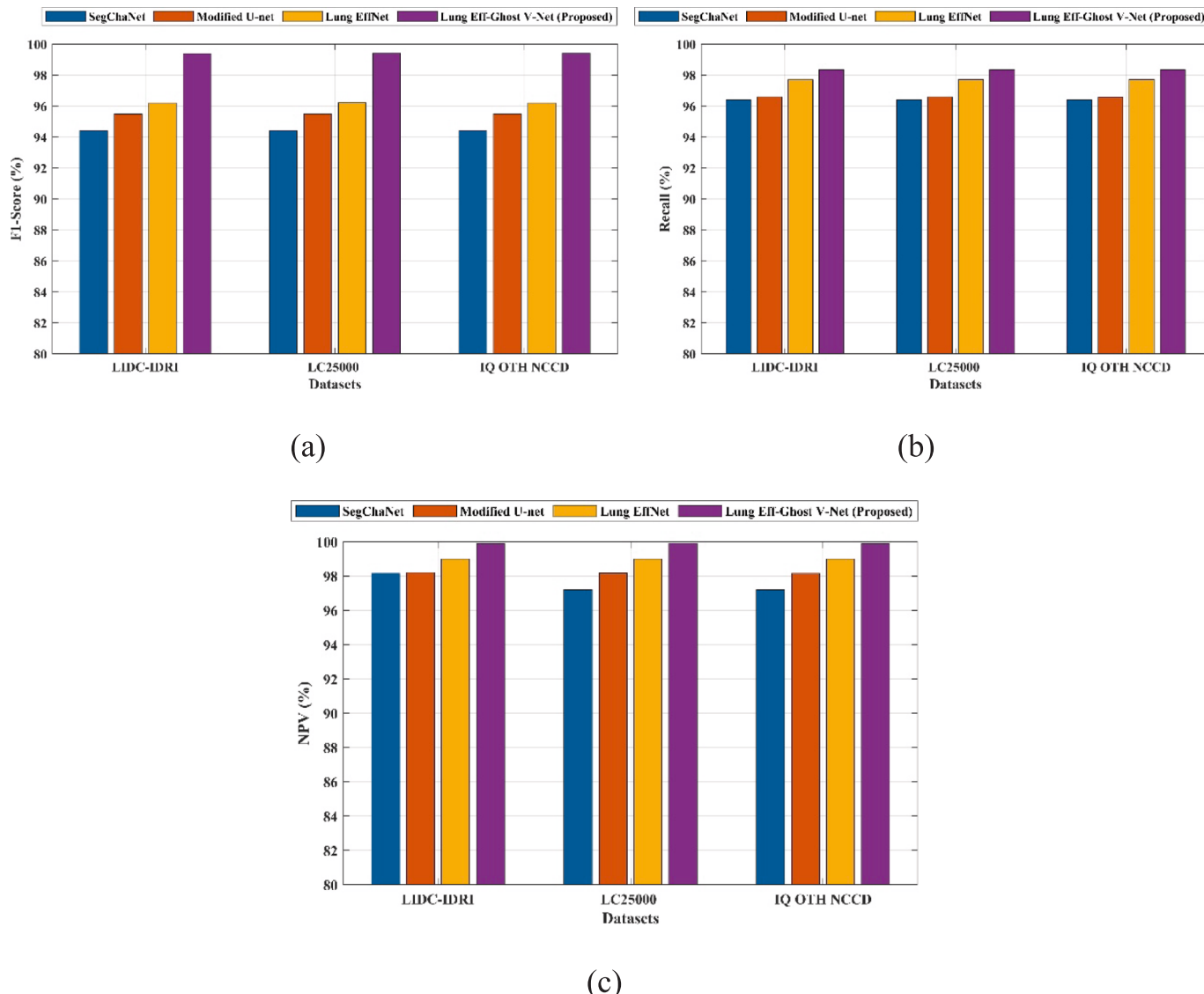


Fig. 8. Performance evaluation of (a) F1-Score, (b) Recall and (c) NPV.

specificity as well and SegChaNet, Modified U-Net, and Lung Eff-Net reached respectively 97.3 %, 97.51 %, and 98.11 % respectively. The graphical analysis for the various performance metrics like F1-score, Recall and NPV is shown in the Fig. 8(a)–(c).

A higher F1-Score refers to a higher precision in both positive cases and lower false positives. The Proposed Lung Eff-Ghost V-Net has been proved to be consistently higher than all other models for each of the three datasets, demonstrating its superiority in the ability to detect lung nodules. For LIDC-IDRI dataset, the Lung Eff-Ghost V-Net achieves an outstanding F1-Score of 99.4 %, far surpassing SegChaNet, Modified U-Net, and Lung EffNet. Similarly, on the LC25000 dataset, it leads with an F1-Score of 99.41 %, outperforming SegChaNet of 94.41 %, Modified U-Net 95.51 %, and Lung EffNet of 96.21 %. On the IQ-OTH/NCCD dataset, proposed model once again attains 99.41 %, while the other models score 94.41 %, 95.51 %, and 96.2 %, respectively. Recall, which represents the proportion of real lung nodules that the model successfully detects, is a crucial parameter that assesses a model's capacity to accurately identify positive cases. In this case, the proposed Lung Eff-Ghost V-Net model consistently demonstrates superior recall performance across all three datasets, achieving 98.33 % recall on LIDC-IDRI dataset, 98.34 % on LC25000 dataset, and 98.33 % on the IQ-OTH/NCCD dataset compared to all other techniques. NPV measures the

rate of correctness for the negative predictions such as how well the model can recognize the absence of a lung nodule. The results obtained through experiment show that the performance of Lung Eff-Ghost V-Net is the best, achieving 99.9 % NPV on the LIDC-IDRI dataset, which accounts for its excellent negative case detection capability. It performs better than the other models, such as SegChaNet with 98.15 %, Modified U-net with 98.2 %, and Lung EffNet with 99 %. Additionally, in the LC25000 dataset, the Lung Eff-Ghost V-Net again emerges at the top NPV of 99.91 % in comparison to other models. In the IQ-OTH/NCCD, Lung Eff-Ghost V-Net acquired highest NPV of 99 %. The graphical analysis for the various performance metrics like FPR, FNR and MCC is shown in the Fig. 9(a)–(c).

The proposed Lung Eff-Ghost V-Net model outperforms the other ones with the minimum FPR of 0.016 for the LIDC-IDRI dataset, implying that it gives the least number of false positive. Comparing with other models, FPR is 0.036 by SegChaNet, Modified U-net achieves its FPR at 0.027, and Lung EffNet reduced the FPR to 0.023. For the LC25000 dataset, Lung Eff-Ghost V-Net had achieved the lowest FPR at 0.01, which was seen to be much lower than SegChaNet with 0.05, Modified U-net at 0.04, and Lung EffNet at 0.03. The IQ-OTH/NCCD dataset follows the same pattern, with the Lung Eff-Ghost V-Net again demonstrating the lowest FPR of 0.01. FNR measures the percentage of

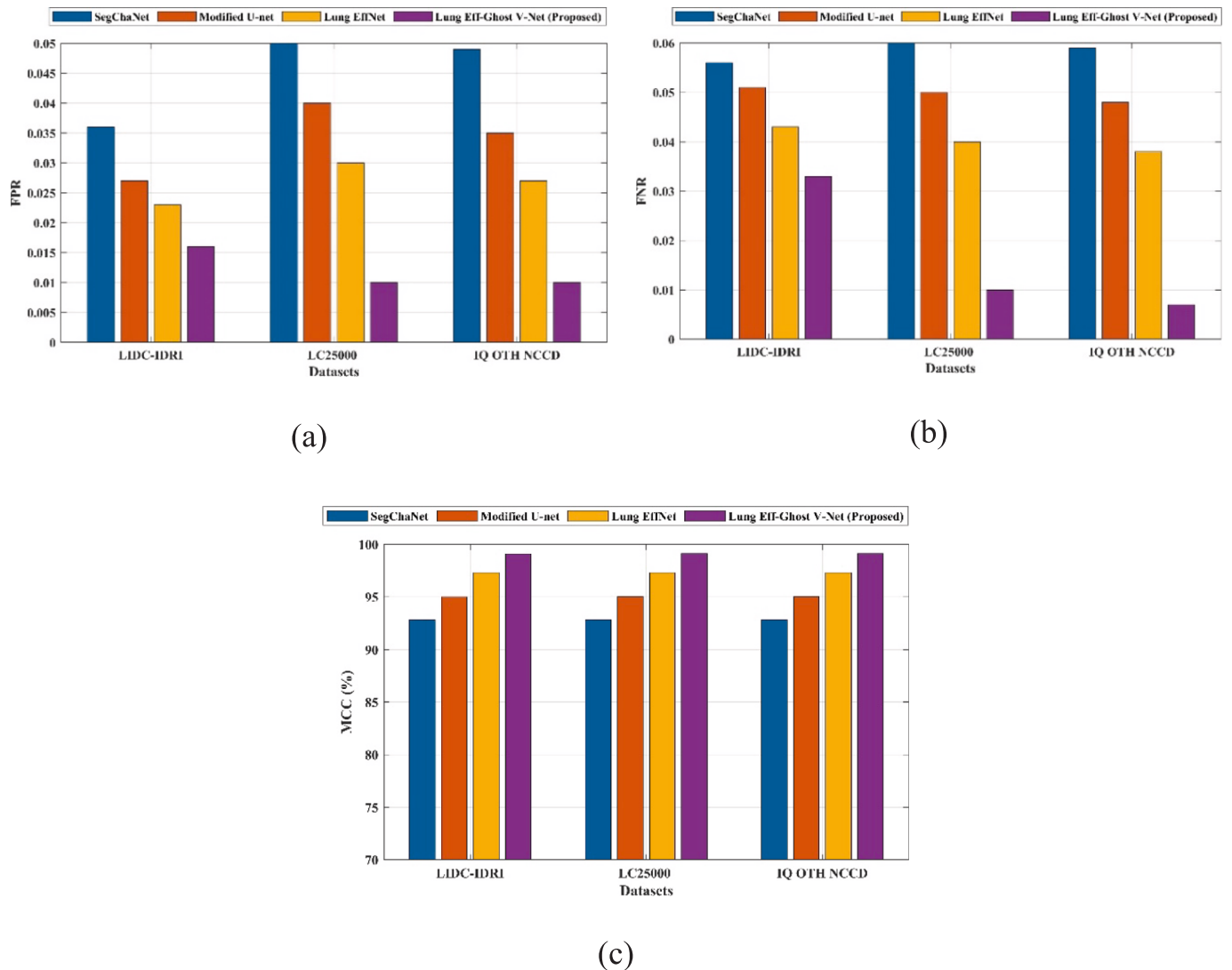


Fig. 9. Performance evaluation of (a) FPR, (b) FNR and (c) MCC.

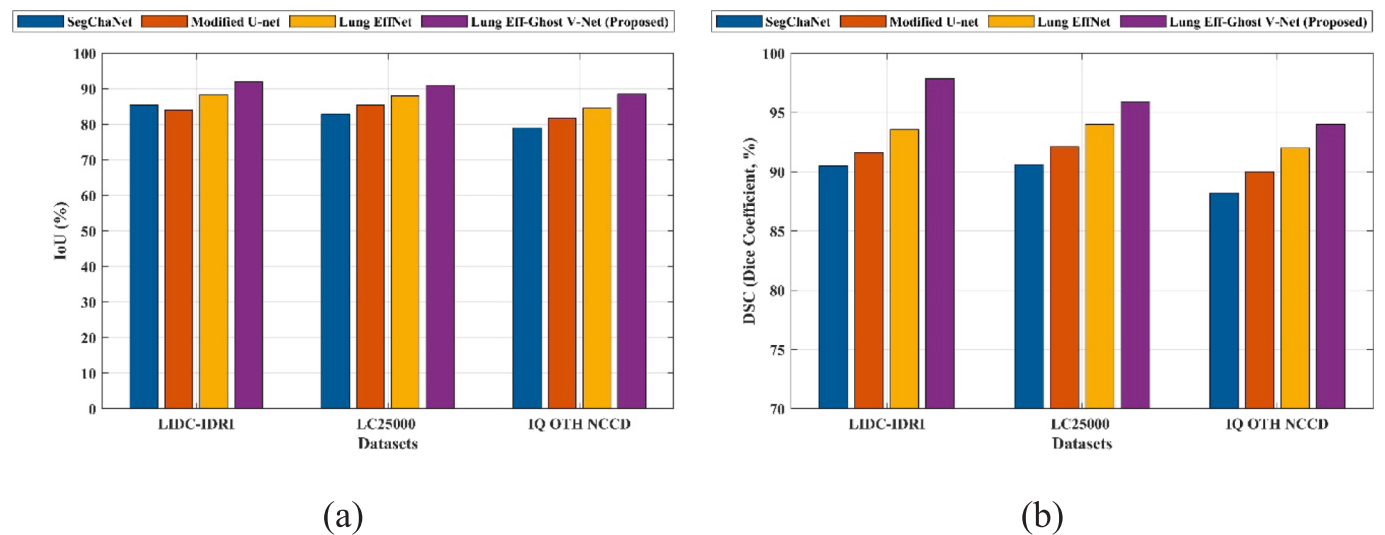


Fig. 10. Performance evaluation of (a) IoU and (b) DSC.

Table 1
Ablation study analysis.

Metrics	Eff-Ghost	Eff-Ghost without NDAM	Eff-Ghost with NDAM
IoU	87.2	84.5	90.2
DSC	93	91	95.8
Sensitivity	98.55	99.04	99.27
Specificity	98.75	98.97	99.09
Accuracy	98.64	99.12	99.56
Precision	98.44	98.79	98.98
Recall	97.32	97.81	98.28
F1-Score	98.65	98.88	99.37
NPV	99.52	99.86	99.88
FPR	0.027	0.023	0.016
FNR	0.051	0.043	0.033
MCC	98.63	98.82	99.07

actual lung nodules that are incorrectly classified as negative, meaning a lower FNR indicates better model performance in detecting true positives, or fewer missed cases.

The Lung Eff-Ghost V-Net model consistently achieves the lowest FNR across all three datasets. For the LIDC-IDRI dataset, it records the lowest FNR of 0.033, missing just 3.3 % of the nodules. In the LC25000 dataset, it further improves with an FNR of 0.01, missing only 1 % of the nodules. The IQ OTH NCCD dataset shows the most significant

improvement, with the proposed model achieving an FNR of 0.007, missing just 0.7 % of the nodules, the lowest among all models. In comparison, SegChaNet has the highest FNR across all datasets, missing 5.6 % of nodules in LIDC-IDRI, 6 % in LC25000, and 5.9 % in IQ OTH NCCD. Modified U-net and Lung EffNet show intermediate performance, with progressively lower FNRs compared to SegChaNet, but they still fall short of the proposed model's accuracy. The proposed Lung Eff-Ghost V-Net consistently outperforms the other models across all datasets, achieving MCC values of 99.1 % for LIDC-IDRI, 99.11 % for LC25000, and 99.11 % for IQ OTH NCCD, indicating nearly perfect prediction accuracy. This suggests that the proposed model has the highest correlation between its predictions and the true outcomes, making it highly effective in detecting lung nodules. The graphical analysis for the performance metrics like IoU and DSC is shown in the Fig. 10(a) and (b).

The IoU indicates overlapping areas between the true ground truths and predicted segmentation region, and higher values thus indicate better segmentation performance. For LIDC-IDRI dataset, it shows SegChaNet achieved 85.44 % which shows moderate performance; however, the Modified U-net performed slightly worse with 84.04 %. Lung EffNet achieves an IoU of 88.38 %. In this case, the proposed Lung Eff-Ghost V-Net brings in the highest IoU at 92.05 %, besides which has a good segmentation performance. In LC25000, the same trend persists with SegChaNet at 82.8 %, Modified U-net at 85.5 %, and Lung EffNet at

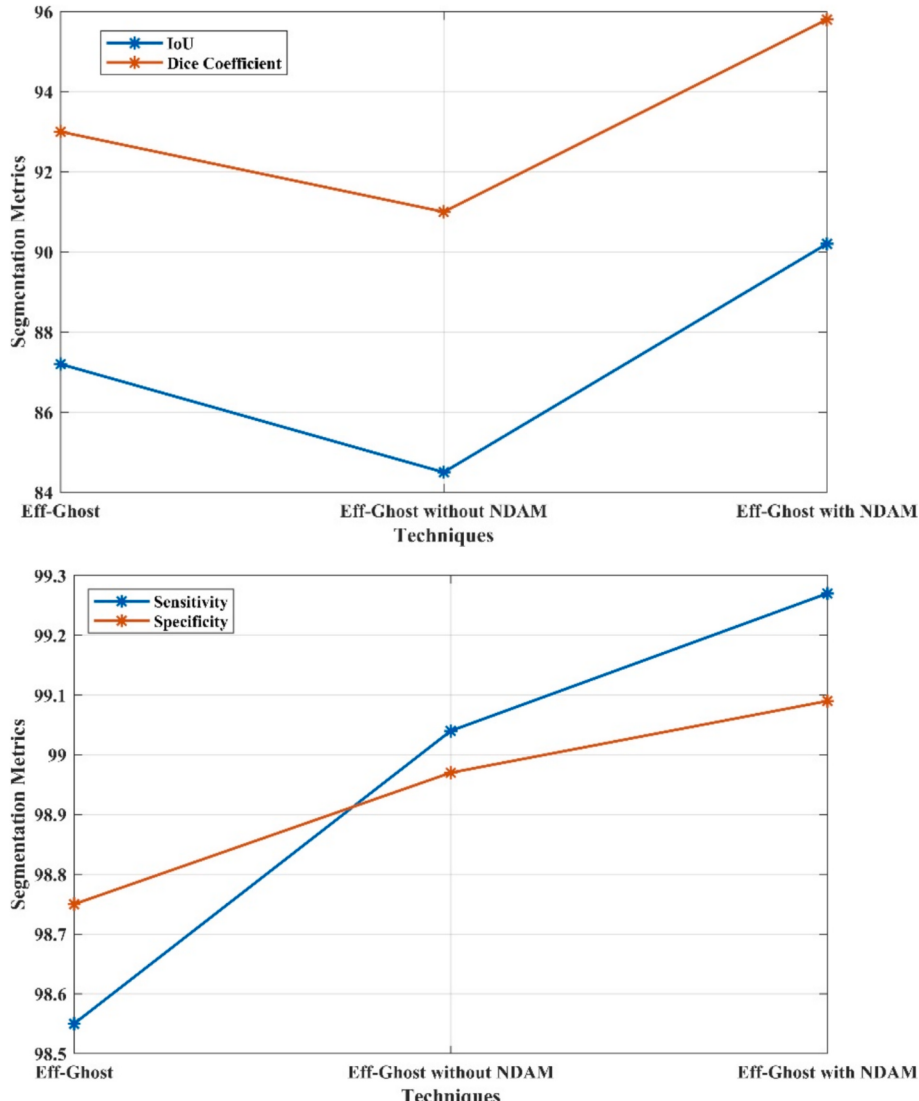


Fig. 11. (a). Ablation analysis of IoU and DSC. **(b).** Ablation analysis of Sensitivity and Specificity.

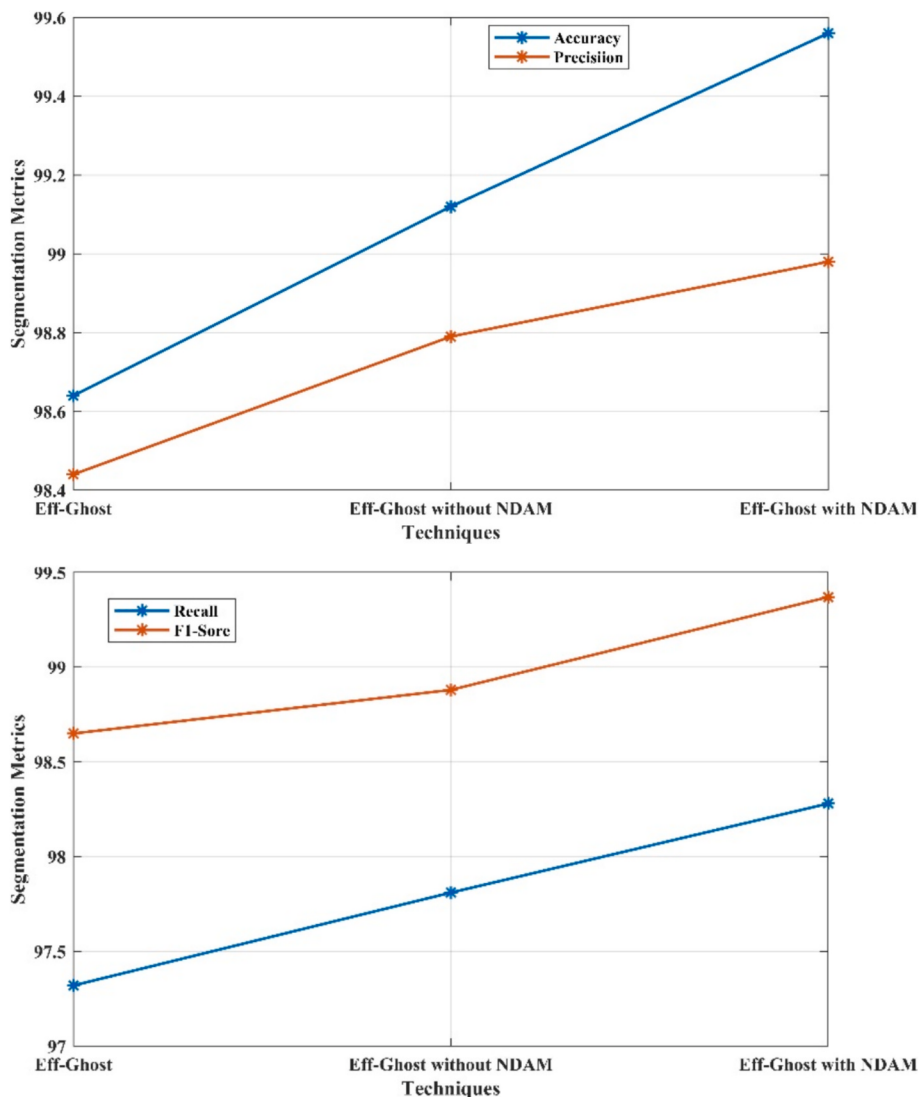


Fig. 12. (a). Ablation analysis of Accuracy and Precision. **(b).** Ablation analysis of F1-score and Recall.

88 %. Here, the Lung Eff-Ghost V-Net takes the lead at an IoU of 91 %. For the IQ OTH NCCD dataset, the lowest IoU is obtained with Seg-ChaNet at 79 %, and improved up to 81.8 % for Modified U-net and 84.5 % for Lung EffNet. The proposed Lung Eff-Ghost V-Net excels with an IoU of 88.5 % and the best performance over all models.

For the LIDC-IDRI dataset, SegChaNet scores 90.49 %, Modified U-net scores 91.62 %, Lung EffNet achieves 93.55 %, and the proposed Lung Eff-Ghost V-Net leads with 97.87 % of DSC. In the LC25000 dataset, SegChaNet scores 90.6 %, Modified U-net reaches 92.1 %, Lung EffNet achieves 94 %, and Lung Eff-Ghost V-Net again performs the best with 95.9 % of DSC. For IQ OTH NCCD, SegChaNet scores 88.2 %, Modified U-net achieves 90 %, Lung EffNet scores 92 %, and the proposed Lung Eff-Ghost V-Net leads with 94 %. Overall, the Lung Eff-Ghost V-Net consistently outperforms the other models, with the highest DSC values of 97.87 %, 95.9 %, and 94 % for LIDC-IDRI, LC25000, and IQ OTH NCCD, respectively, indicating its superior performance in accurately segmenting lung nodules.

4.4. Ablation study analysis

The ablation study is investigated on the proposed model for the various metrics on the baseline model of Eff-Ghost, Eff-Ghost without NDAM and Eff-Ghost with NDAM highlighting the effectiveness of this

integrated approach is illustrated in the Table 1.

For IoU, the highest value was reached by Eff-Ghost at 87.2 %, and the version without NDAM is lower by 3 % points at 84.5 %. The highest value of IoU is achieved for Eff-Ghost with NDAM at 90.2 %, best indicating overlap across predicted and actual lung nodule areas. Similar to DSC, Eff-Ghost reached a high value at 93 %, followed by the slightly lower value of 91 % for the version without NDAM. The Eff-Ghost with NDAM outperforms both versions, providing the highest DSC at 95.8 %, which shows good performance in terms of segmentation accuracy for target regions. These results depict significant improvements in segmentation accuracy that result from models including NDAM within them. The Eff-Ghost model achieves a sensitivity of 98.55 %, while the Eff-Ghost without NDAM reaches 99.04 %, and the Eff-Ghost with NDAM shows the highest sensitivity at 99.27 %. This indicates that the model with NDAM is the best at detecting true positive cases, minimizing false negatives. On the other hand, specificity, or True Negative Rate, evaluates proportion of actual negative cases correctly recognized. Eff-Ghost model has a specificity of 98.75 %, while the Eff-Ghost without NDAM performs slightly better at 98.97 %, and the version with NDAM reaches the highest specificity of 99.09 %. These results demonstrate that the Eff-Ghost with NDAM outperforms the other models in correctly identifying negative cases, reducing false positives. The corresponding graphical analysis for this ablation study

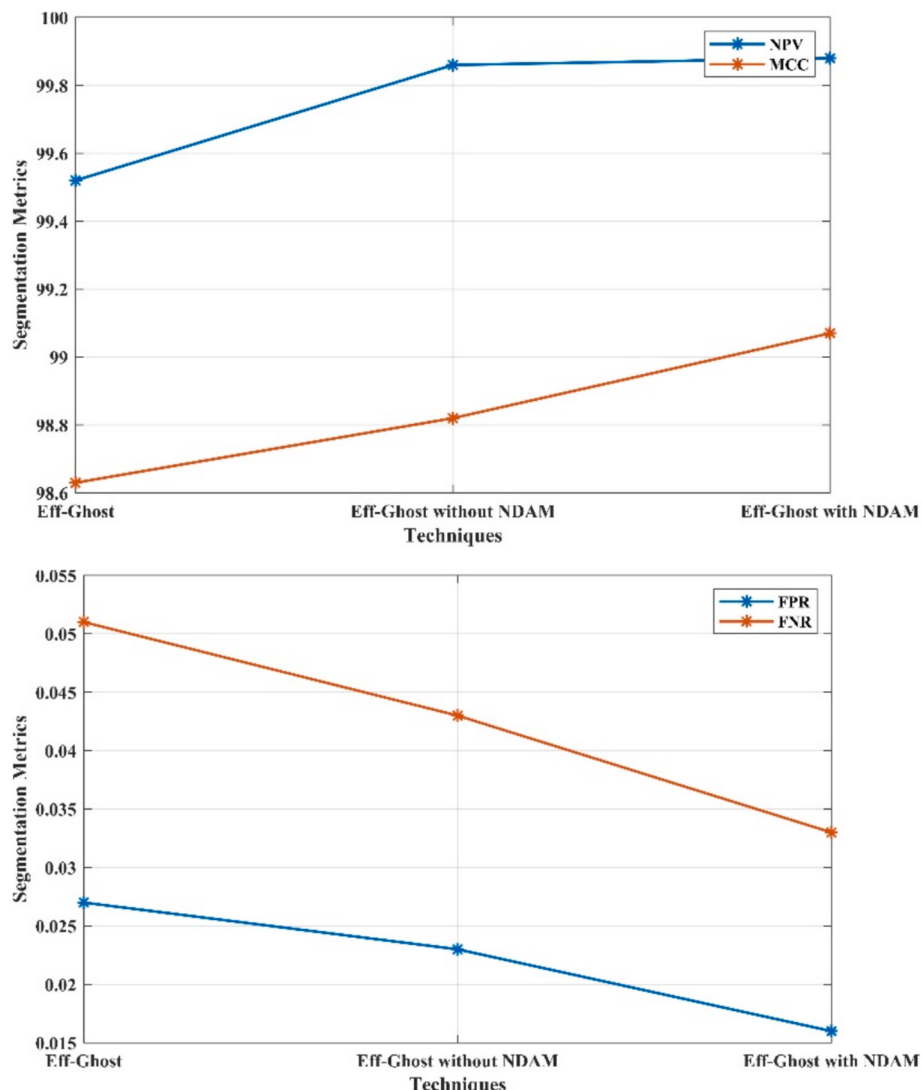


Fig. 13. (a). Ablation analysis of NPV and MCC. (b). Ablation analysis of FPR and FNR.

for metrics IoU, DSC and Sensitivity and Specificity are depicted in the Fig. 11(a) and (b) respectively.

The accuracy of the best model is Eff-Ghost at 98.64 % with that model which does not include NDAM being a little better with an accuracy of 99.12 %. However, the overall best is still when using Eff-Ghost with NDAM at 99.56 %. The precision of the Eff-Ghost has 98.44 %, the one without NDAM showed to have 98.79 %, and Eff-Ghost with NDAM again leads with 98.98 %. This highlights the ability of the Eff-Ghost with NDAM to minimize false positive predictions, making it the most precise model in identifying true positives. The Eff-Ghost model achieves 97.32 % recall, and the other model lacking NDAM performs a bit better at 97.81 %, but again, the Eff-Ghost with NDAM seems to outperform them both in terms of achieving 98.28 % recall and its capability to detect more true positive cases. In terms of F1 Score, which is harmonic mean of recall and precision, the Eff-Ghost model scores at 98.65 %, the one without NDAM scores at 98.88 %, and the Eff-Ghost with NDAM scores at F1 Score of 99.37 %. The corresponding graphical analysis for this ablation study for metrics Precision, Accuracy, and F1-score, Recall, are depicted in the Fig. 12(a) and (b) respectively.

NPV of Eff-Ghost model is 99.52 % compared to that of the version without NDAM, which is at 99.86 %. The highest NPV of the Eff-Ghost with NDAM is 99.88 %, correspondingly to its capacity to avoid false negative predictions. As for MCC, it pertains to quality measurements

concerning binary classifications where the performance of the Eff-Ghost model was at 98.63 % whereas the model without NDAM might result to 98.82 %. As with the previous case, the Eff-Ghost with NDAM takes the lead again with MCC of 99.07 %, denoting better overall classification performance. The FPR of the Eff-Ghost is 0.027; but the version of the model not including NDAM finds slightly better results at 0.023. The best score is by the Eff-Ghost with NDAM at an FPR of 0.016, indicating this technique can correctly classify true negative cases. The FNR of the Eff-Ghost model is 0.051. Without NDAM, it performs at 0.043. And again, the Eff-Ghost with NDAM has the lowest FNR of 0.033, which indicates that it misclassifies fewer positive cases. The corresponding graphical analysis for this ablation study for metrics NPV, MCC and FPR, FNR are depicted in the Fig. 13(a) and (b) respectively.

5. CONCLUSION

The proposed Lung EffGhost V-Net model significantly enhances the segmentation and detection accuracy of lung cancer (LC) from CT images by integrating EfficientNet, GhostNet, and V-Net into a unified deep learning framework. This hybrid architecture improves computational efficiency while maintaining high segmentation precision. The model incorporates a novel deep attention mechanism (NDAM) that enables it to suppress irrelevant background regions and focus on critical lung nodule features, enhancing feature refinement during decoding.

Additionally, the Pyramid Attention Network (PAN) is employed to perform multi-scale detection, improving the identification of nodules of varying sizes and shapes. To further boost segmentation performance, an Improved Gaussian Filter (IGF) based on a Logistic Chaotic Map is utilized during preprocessing to adaptively reduce noise while preserving essential edges and textures. Extensive experiments conducted on three benchmark datasets—LIDC-IDRI, LC25000, and IQ-OTH/NCCD—demonstrate that the proposed model achieves superior performance with 99.6 % accuracy, 97.87 % Dice Similarity Coefficient (DSC), and 92.05 % Intersection over Union (IoU), outperforming existing methods such as SegChaNet, Modified U-Net, and Lung EffNet. These results indicate that the Lung EffGhost V-Net model is robust, generalizable, and effective across varied clinical imaging scenarios. Future enhancements could involve extending the model to incorporate additional imaging modalities such as PET scans for improved diagnostic precision. Moreover, real-time deployment using edge computing technologies could be explored to support faster diagnosis in low-resource or point-of-care environments.

CRediT authorship contribution statement

T. Sujatha: Conceptualization. **P.D. Mahendhiran:** Writing – review & editing, Supervision. **Esther Daniel:** Writing – review & editing, Supervision.

Funding

On Behalf of all authors the corresponding author states that they did not receive any funds for this project.

Declaration of competing interest

The authors declare that they have no known competing financial interests or personal relationships that could have appeared to influence the work reported in this paper.

Data availability

No data was used for the research described in the article.

REFERENCES

- [1] D. Bhattacharyya, N. Thirupathi Rao, E.S.N. Joshua, Y.C. Hu, A bi-directional deep learning architecture for lung nodule semantic segmentation, Vis. Comput. 39 (11) (2023) 5245–5261.
- [2] S.R.R. BR, S. Sen, R. Bhatt, M.L. Dhanetwal, M. Sharma, R. Naaz, Stacked neural nets for increased accuracy on classification on lung cancer, Meas.: Sens. 32 (2024) 101052.
- [3] Y. Chen, X. Hou, Y. Yang, Q. Ge, Y. Zhou, S. Nie, A novel deep learning model based on multi-scale and multi-view for detection of pulmonary nodules, J. Digit. Imaging 36 (2) (2023) 688–699.
- [4] M.A. Cifci, SegChaNet: a novel model for lung cancer segmentation in CT scans, Appl. Bionics Biomech. 2022 (1) (2022) 1139587.
- [5] L.J. Crasta, R. Neema, A.R. Pais, A novel Deep Learning architecture for lung cancer detection and diagnosis from Computed Tomography image analysis, Healthcare Anal. 5 (2024) 100316.
- [6] S. Gite, A. Mishra, K. Kotecha, Enhanced lung image segmentation using deep learning, Neural Comput. Appl. 35 (31) (2023) 22839–22853.
- [7] A. Gopinath, P. Gowthaman, M. Venkatachalam, M. Saroja, Computer aided model for lung cancer classification using cat optimized convolutional neural networks, Meas.: Sens. 30 (2023) 100932.
- [8] V.K. Gugulothu, S. Balaji, An early prediction and classification of lung nodule diagnosis on CT images based on hybrid deep learning techniques, Multimed. Tools Appl. 1 (2024).
- [9] M. Imran, B. Haq, E. Elbasi, A.E. Topcu, W. Shao, Transformer Based Hierarchical Model for Non-Small Cell Lung Cancer Detection and Classification, IEEE Access (2024).
- [10] Z. Ji, J. Zhao, J. Liu, X. Zeng, H. Zhang, X. Zhang, I. Ganchev, ELCT-YOLO: an efficient one-stage model for automatic lung tumor detection based on CT images, Mathematics 11 (10) (2023) 2344.
- [11] Z. Ji, Z. Zhao, X. Zeng, J. Wang, L. Zhao, X. Zhang, I. Ganchev, ResDSda_U-Net: A novel U-Net based residual network for segmentation of pulmonary nodules in lung CT images, IEEE Access (2023).
- [12] R. Mahum, A.S. Al-Salman, Lung-RetinaNet: Lung cancer detection using a RetinaNet with multi-scale feature fusion and context module, IEEE Access 11 (2023) 53850–53861.
- [13] T.I. Mohamed, O.N. Oyelade, A.E. Ezugwu, Automatic detection and classification of lung cancer CT scans based on deep learning and ebola optimization search algorithm, PLoS One 18 (8) (2023) e0285796.
- [14] I. Naseer, S. Akram, T. Masood, M. Rashid, A. Jaffar, Lung cancer classification using modified U-Net based lobe segmentation and nodule detection, IEEE Access 11 (2023) 60279–60291.
- [15] N.E. Protonotarios, I. Katsamenis, S. Sykiotis, N. Dikaios, G.A. Kastis, S. N. Chatzioannou, A. Doulamis, A few-shot U-Net deep learning model for lung cancer lesion segmentation via PET/CT imaging, Biomed. Phys. Eng. Express 8 (2) (2022) 025019.
- [16] K. Ramana, M.R. Kumar, K. Sreenivasulu, T.R. Gadekallu, S. Bhatia, P. Agarwal, S. M. Idrees, Early prediction of lung cancers using deep saliency capsule and pre-trained deep learning frameworks, Front. Oncol. 12 (2022) 886739.
- [17] R. Raza, F. Zulfiqar, M.O. Khan, M. Arif, A. Alvi, M.A. Iftikhar, T. Alam, Lung-EffNet: Lung cancer classification using EfficientNet from CT-scan images, Eng. Appl. Artif. Intel. 126 (2023) 106902.
- [18] Z. Riaz, B. Khan, S. Abdullah, S. Khan, M.S. Islam, Lung tumor image segmentation from computer tomography images using MobileNetV2 and transfer learning, Bioengineering 10 (8) (2023) 981.
- [19] Y. Said, A.A. Alsheikhly, T. Shawly, H. Lahza, Medical images segmentation for lung cancer diagnosis based on deep learning architectures, Diagnostics 13 (3) (2023) 546.
- [20] A. Su, F.R. Pp, A. Abraham, D. Stephen, Deep learning-based BoVW-CRNN model for lung tumor detection in nano-segmented CT images, Electronics 12 (1) (2022) 14.
- [21] M. Tsivgoulis, T. Papastergiou, V. Megalooikonomou, An improved SqueezeNet model for the diagnosis of lung cancer in CT scans, Mach. Learn. Appl. 10 (2022) 100399.
- [22] S. Wankhade, S. Vigneshwari, A novel hybrid deep learning method for early detection of lung cancer using neural networks, Healthcare Anal. 3 (2023) 100195.
- [23] B.E. Youssef, A. Alksas, A. Shalaby, A.H. Mahmoud, E. Van Bogaert, N.S. Alghamdi, A. El-Baz, Integrated deep learning and stochastic models for accurate segmentation of lung nodules from computed tomography images: a novel framework, IEEE Access 11 (2023) 99807–99821.
- [24] F. Zhang, Q. Wang, E. Fan, N. Lu, D. Chen, H. Jiang, Y. Yu, Enhancing non-small cell lung cancer tumor segmentation with a novel two-step deep learning approach, J. Radiat. Res. Appl. Sci. 17 (1) (2024) 100775.
- [25] G. Zhang, Z. Yang, S. Jiang, Automatic lung tumor segmentation from CT images using improved 3D densely connected UNet, Med. Biol. Eng. Compu. 60 (11) (2022) 3311–3323.